

Multiple Quantum Phase Transitions at the superconducting LaTiO₃/SrTiO₃ interface

J. Biscaras¹, N. Bergeal¹, S. Hurand¹, C. Feuillet-Palma¹, A.

Rastogi², R. C. Budhani^{2,3}, M. Grilli⁴, S. Caprara⁴, J. Lesueur¹

¹*LPEM- UMR8213/CNRS - ESPCI ParisTech - UPMC, 10 rue Vauquelin - 75005 Paris, France*

²*Condensed Matter - Low Dimensional Systems Laboratory, Department of Physics,
Indian Institute of Technology Kanpur, Kanpur 208016, India*

³*National Physical Laboratory, New Delhi - 110012, India and*

⁴*Istituto Nazionale per la Fisica della Materia, Unità di Roma 1 and SMC Center,
and Dipartimento di Fisica Università di Roma “La Sapienza”, piazzale Aldo Moro 5, I-00185 Roma, Italy*

(Dated: June 22, 2021)

We study the magnetic field driven Quantum Phase Transition (QPT) in electrostatically gated superconducting LaTiO₃/SrTiO₃ interfaces. Through finite size scaling analysis, we show that it belongs to the (2+1)D XY model universality class. The system can be described as a disordered array of superconducting islands coupled by a two dimensional electron gas (2DEG). Depending on the 2DEG conductance tuned by the gate voltage, the QPT is single (corresponding to the long range phase coherence in the whole array) or double (one related to local phase coherence, the other one to the array). By retrieving the coherence length critical exponent ν , we show that the QPT can be “clean” or “dirty” according to the Harris criteria, depending on whether the phase coherence length is smaller or larger than the island size. The overall behaviour is well described by a theoretical approach of Spivak *et al.*, in the framework of the fermionic scenario of 2D superconducting QPT.

Two-dimensional electron gas at the interface between insulating oxides (O-2DEG) have raised considerable interest[1–3]. Indeed, they display very high mobilities suitable for applications[4], but also a rich phase diagram, with different quantum ground states such as magnetism[5–8] or superconductivity[9, 10] for example. Moreover, these properties can be finely tuned using a gate voltage[11, 12]. Therefore, O-2DEG appear as interesting systems to study Quantum Phases Transitions (QPT) that occur between different quantum states, when a parameter in the Hamiltonian crosses over a critical value[13]. The critical behaviour of the observables belong to universality classes which depend on general properties of the system such as its dimensionality or its symmetries, and not on the microscopic details. The associated critical exponents obey specific rules, among which the so-called “Harris criteria”. The latter stipulates that the correlation length exponent ν must satisfy $\nu \geq 2/d$ for “dirty” disordered systems and $\nu \leq 2/d$ for “clean” ones, where d is the spatial dimensionality[14].

An important example of QPT is the transition from a superconducting to an insulating state in two dimensions, which has been a matter of debate for a long time[15]. Numerous experiments with contrasted results[15] have been performed, and a large variety of critical exponents have been found. The nature of the non-superconducting state and the role of the disorder are still unclear. The possibility of observing multiple QPT has been raised recently[16–18]. Here we show that a perpendicular magnetic field applied on a superconducting O-2DEG drives the system towards a weakly localized metal. We evidence two QPT corresponding to the “dirty” and “clean” limits of the Harris criteria, which can be controlled by the gate voltage. More precisely, we have shown that the QPT in

superconducting O-2DEG belongs to the (2+1)D XY universality class[13], and follows a fermionic scenario[19, 20]. Finite size scaling analysis (FSS) reveals that depending on the gate voltage and the temperature, the product of the critical exponents $z\nu$ (z is the dynamical exponent) is $z\nu = 2/3$ in the clean regime in agreement with calculations[21], and greater than one otherwise, as expected from the Harris criteria. We argue that this multiple QPT can be understood in the frame of a recent model developed by Spivak *et al.*[17] to describe the QPT in a disordered array of superconducting puddles coupled by a 2DEG. This result demonstrates that the superconducting O-2DEG tunability is a powerful tool to study fundamental properties of superconductors in low dimensions. We anticipate that further insight within QPT involving two dimensional superconductors will emerge. For example, the role of disorder and inhomogeneity[17, 22], Coulomb repulsion, charge fluctuations and screening on the QPT[23–25] can be explored in more details.

The LaTiO₃/SrTiO₃ epitaxial interface exhibits a high mobility O-2DEG which displays superconductivity[10]. We recently showed that T_c can be tuned by electrostatic gating from its maximum value of ~ 200 mK to zero, and that superconductivity coincides with the presence of Highly Mobile Carriers (HMC) at the edge of the quantum well formed by the O-2DEG at the interface[12]. It is therefore possible to prepare the system with a given T_c by controlling the gate voltage V_G (inset Fig. 1a), and to study how the superconducting state is destroyed by a perpendicular magnetic field in this situation. Samples are grown by pulsed laser deposition of 15 unit cells of LaTiO₃ on TiO₂-terminated (001)SrTiO₃ substrate (see Biscaras *et al.*[10] for details). A metallic back gate is evaporated at the rear of the 500 μm thick SrTiO₃ substrate and connected to a voltage source (V_G). Standard four-probe resistance measurements are made with a current sufficiently low to avoid any heating of the electron at the lowest temperature. The polarization scheme described previously[26] is applied to insure a reversible behaviour of the superconducting O-2DEG. The normal state displays the logarithmic temperature dependence of the conductivity, characteristic of weak localization in two dimensions[10]. Hence, the magnetic field turns the 2D superconductor into a 2D weakly localizing metal as shown in Fig. 1a for $V_G = +80$ V, where the resistance per square R_S is plotted as a function of temperature T for different perpendicular magnetic fields B . A close-up view of the data reveals a critical field B_\times which separates the two regimes, and for which R_S is constant (Fig. 1b). The same set of data plotted as R_S versus B for different temperatures in Fig. 2a displays a crossing point ($R_\times = 372.4 \Omega/\square$, $B_\times = 0.185$ T) where the resistivity does not depend on temperature. This is a first signature of a continuous QPT.

In such zero temperature transitions, the ground state of the Hamiltonian is changed by an external parameter (for now magnetic field). Close to the transition the correlation length ξ in the space dimensions and the dynamical correlation length ξ_τ in the imaginary time dimension of the quantum fluctuations diverge with a power law dependence of the distance from the transition $\delta = |B - B_\times|$ [13, 15]. At $T=0$ the correlation length exponent ν defined as $\xi \propto |\delta|^{-\nu}$ and the dynamical scaling exponent z defined as $\xi_\tau \propto \xi^z$ are believed to be independent of the microscopic details of the transition and only depend on few properties of the system, such as the dimensionality and the range of the interactions, which define universality classes for the QPT[13]. The effective dimensionality of the system is $d + z$ where d is the spatial dimensionality. At finite temperature, the imaginary time dimension is limited by the temperature fluctuations so that the dimensionality of the system is $d + z$ at $T=0$ only, and d at finite temperature[15]. More precisely, the finite temperature limits the size of the temporal direction by the thermal cut-off $L_\tau = \hbar/k_B T$ which is now an upper bound for the dynamical correlation length ξ_τ near the critical point. It follows that in the

spatial dimensions the quantum fluctuations lose phase coherence over a temperature dependent dephasing length $L_\phi \propto 1/T^{1/z}$ [13]. This leads to a so-called finite size scaling (FSS) of the observables of the system. For instance, the resistance takes the form :

$$\frac{R_S}{R_\times} = F\left(\frac{|B - B_\times|}{T^{1/z\nu}}\right) \quad (1)$$

where F is a universal function with $F(0)=1$ [27]. The critical exponents can then be retrieved by a scaling procedure[15] as follows. The resistance is rewritten as $R(\delta, t) = R_\times F(|\delta|t)$ with t an unknown parameter that depends only on T . The parameter t is then found at each temperature T by optimizing the collapse around the critical point between the curve $R(\delta, t(T))$ at temperature T and the curve $R(\delta, t(T_0))$ at the lowest temperature considered T_0 , with $t(T_0)=1$. The dependence of t with temperature should be a power law of the form $t = (T/T_0)^{-1/z\nu}$ in order to have a physical sense, thus giving the critical exponent product $z\nu$. The interest of this procedure is to perform the scaling without knowing the critical exponent beforehand. The result of this procedure applied to the data displayed in Fig. 1a shows that data collapse onto a single (bi-valued) curve in Fig. 2b, and yields $z\nu=0.66$ (inset Fig. 2b).

In the literature, $z\nu=2/3$ has been observed for perpendicular magnetic field driven transitions in conventional 2D disordered superconductors such as a-NbSi[28, 29] or a-Bismuth[15, 30]. This value corresponds to the “clean” (2+1)D XY universality class according to numerical simulations[21, 31, 32], where the extra dimension refers to the imaginary time in the quantum transition[13]. In that case, long range superconducting correlations are destroyed by quantum phase fluctuations. In general, the dynamical exponent z is found to be one, corresponding to long range Coulomb interaction between charges[13, 27], as it has been measured in a-MoGe for instance[20]. In the absence of specific screening or dissipation mechanism[33], there is no reason to invoke short range interactions which would set $z \neq 1$ [34]. Therefore, if $z = 1$, then $\nu = 2/3$, which means that $\nu \leq 2/d$, with the spatial dimension $d = 2$. According to the very general Harris criteria[14], the system is in the “clean” limit at the relevant scale for the transition, namely the dephasing length L_ϕ . In 2D disordered systems, i.e. in the “dirty” regime, ν is expected to increase beyond 1[31, 32], following the Harris criteria, as observed in a-MoGe[20], InOx[35] or ultra-thin High Tc superconductors[36] for instance.

We now focus on the same R_S vs T curves below 0.1 K ($V_G = +80$ V). A blow-up in Fig. 1c evidences another critical field B_C for which the resistance is constant in a restricted range of temperature and $\frac{\partial R}{\partial T}$ changes sign. Reported on Fig. 2c, R_S vs B curves display a crossing point ($B_C=0.235$ T, $R_C=376.6$ Ω/\square), and the FSS analysis shows a good collapse of the curves, leading to a critical exponent product $z\nu=1.5$ (Fig. 2d). This is clearly greater than one. The system is in the dirty limit of the Harris criteria at the scale L_ϕ . As a conclusion for $V_G = +80$ V, the system undergoes a “clean” QPT ($z\nu=2/3$) whose critical behaviour can be seen between 120 mK and 220 mK, and a “dirty” QPT ($z\nu=3/2$) at lower temperature.

When the gate voltage is tuned to lower or even negative values, the system is driven toward a more resistive state, and T_c decreases (see inset Fig. 1a). In Fig. 3a, R_S is displayed as a function of the temperature for different magnetic fields and for a gate voltage $V_G = -15$ V. A plateau is clearly seen down to the lowest temperature for a critical field $B_\times=0.1$ T ($R_\times=2176$ Ω/\square), as confirmed by the presence of a crossing point (inset of Fig. 3a). The FSS analysis reveals that two regimes take place as shown in Fig. 3b. Indeed, two distinct $z\nu$ values can be extracted : at “high”

temperature (70 mK to 120 mK) $z\nu=2/3$ and at the lowest temperatures $z\nu=3/2$. The corresponding collapses of the data depicted in Fig. 3c,d confirm the existence of the QPT.

We made the same analysis for all the gate voltages between $V_G = -40$ V and $V_G = +100$ V. The results are presented in Fig. 4. For $V_G \geq +10$ V, two distinct critical fields B_\times and B_C ($B_C > B_\times$) can be found (region II in Fig. 4a), whereas for $V_G \leq +10$ V, they merge into a unique value (region I). Two important observations need to be made : (i) B_\times increases with V_G and then saturates when $B_\times \neq B_C$ to a value B_d . (ii) B_C matches T_c defined as the temperature where the normal state resistance drops of 10% [12]. B_C is therefore the critical field which fully destroys superconductivity in the system. The critical exponent product $z\nu$ extracted from the FSS around both critical fields are reported as a function of V_G in Fig. 4b. $z\nu$ corresponding to B_\times is constant and equals to $2/3$: the QPT is in the clean limit. For B_C , $z\nu$ changes with V_G , with rather important error bars due to the finite scaling range in temperature, but is *always larger than 1*, indicating that the QPT is in the dirty limit.

To account for these observations, we propose the following scenario based on the XY model where superconductivity is destroyed by phase fluctuations in a two-dimensional superconductor. We suppose that the system consists in superconducting islands coupled by non-superconducting metallic regions (see Fig. 5 for a sketch). Indeed, as shown previously [12], the superconducting O-2DEG is made of two types of carriers, a few Highly Mobile Carriers (HMC) and a majority of Low Mobile Carriers (LMC). We argued that the presence of HMC triggers superconductivity in the system. The density of HMC [12] (in the 10^{12} cm $^{-2}$ range) and its evolution with the gate voltage is very similar to the superfluid density directly measured by Bert *et al.* [37] in LaAlO $_3$ /SrTiO $_3$ interfaces. We therefore assume that HMC form the superfluid with intrinsic inhomogeneity due to its very low average density and the associated density fluctuations, and that LMC form the metal which provides long range coupling. The system is therefore described as a disordered array of superconducting puddles of size L_d coupled by a metallic 2DEG. Such a situation has been studied by Spivak, Oreto and Kivelson (SOK) [17]. Superconducting phase coherence is governed by the transport properties of the metallic part through the proximity effect, and depends on the 2DEG conductance G_{2DEG} . If the coupling is strong enough (high G_{2DEG}), puddles can develop full local superconductivity and two phase transitions can be observed corresponding respectively to the puddles themselves and to the disordered array of puddles. In the opposite case (low G_{2DEG}), decoupled puddles are always in a fluctuating regime, and only the full array transition can be seen at low temperature. These two regimes can be observed in LaTiO $_3$ /SrTiO $_3$ interfaces, and the transition from one to the other can be controlled by the gate voltage. Indeed, the conductance $G_S = 1/R_S$ increases with V_G (inset Fig. 1a), and so does the coupling. Region I is therefore the low coupling regime with a single transition ($B_\times = B_C$), whereas region II refers to the high coupling one with two transitions ($B_C > B_\times$). In the later case, B_\times is the critical field for the puddle transition and B_C the one for the whole array : as a consequence T_c scales with B_C as observed experimentally.

The SOK model develops a full analysis of the long range coupling between puddles. They introduce the concept of ‘‘optimal puddle’’ [17] to account for the statistical distribution of puddles sizes, and show that the critical magnetic field B_C scales with the coupling parameter G_{2DEG} . At low conductance, $B_C \propto G_{2DEG}$, whereas as high conductance, $B_C \propto G_{2DEG}^{1/4}$. To test the model in more details, we plotted the critical field B_C as a function of the conductance G_S on a log-scale in Fig. 4c. The data are in good agreement with the theory. Not only the two regimes can be clearly identified, but also the values of the slopes correspond to the calculated one. This is a strong

indication that the SOK model is a good representation of the physics involved in these experiments.

On this basis, we can now analyse the QPT, remembering that the thermal dephasing length $L_\Phi \sim T^{-1/z}$ ($z = 1$ here). A cartoon illustrating the situation is shown in Fig. 5. Let us first focus on region II as defined in Fig. 4. At high temperature, the phase correlation length L_Φ is smaller than the superconducting puddles size L_d , and the intra-puddle physics dominates. The critical field B_\times corresponds to the dephasing field B_d on a puddle of size L_d ($B_d \sim \Phi_0/L_d^2$ where Φ_0 is the flux quantum)[17, 18], and does not depend on the microscopic parameters of the system tuned by V_G . This is why it is constant as a function of V_G ($B_\times = B_d$) as shown in Fig. 4a. From the value of B_d , we can estimate L_d to be of the order of 100 nm. Since $L_\Phi < L_d$, the system is in the clean limit, and $z\nu = 2/3 < 1$ (Fig. 4b) as expected from the Harris criteria. When lowering the temperature, L_Φ crosses L_d at T_d , and the whole array undergoes the transition with a critical field B_C . In that case, phase fluctuations extend over wide disordered regions and the dirty (2+1)D XY model applies ($z\nu > 1$ as shown in Fig. 4b). In region I, only the array displays a transition with a single critical field B_C . However, as the temperature is lowered, L_Φ also crosses L_d , and we therefore observe a transition from a clean ($z\nu = 2/3 < 1$) to a dirty ($z\nu > 1$) (2+1)D XY limit. At this point, it is worthwhile mentioning that, strictly speaking, the transition at B_C is the only true QPT, since the scaling holds down to the lowest temperature. However, at sufficiently high temperature, the transition at B_\times displays fluctuations corresponding also to a real QPT which is never reached. Indeed, the diverging coherence length crosses L_d , which acts as a cut-off length for the intra-puddle physics. B_\times is therefore a crossover field[17], but we consider both transitions as QPT in view of the quantum nature of the fluctuations.

Such an analysis reveals that the tunable LaTiO₃/SrTiO₃ epitaxial interface appears as a unique system to study superconducting QPT in 2D, which is well described by the (2+1)D XY model as expected. The role of disorder on the critical exponents is clearly evidenced, together with the possibility of observing multiple QPT as previously proposed theoretically [16–18]. These models have been developed in the framework of the so-called “fermionic scenario”[19, 20], where superconductivity disappears because Cooper pairs are destroyed, as opposed to the “bosonic scenario”[27], where they localize and form an insulator. In the later case, the QPT takes place for critical resistances R_C close to the quantum resistance $R_Q = h/4e^2 \simeq 6.5 \text{ k}\Omega/\square$, whereas in the former one it can occur at much lower resistances[16–18]. Steiner *et al.*[35] compiled experimental results in the literature and clearly evidenced the two behaviours : the QPT separates a superconducting phase from a weakly localizing metal in the less disordered systems ($R_C \leq R_Q$), and from an insulator in strongly disordered materials ($R_C \sim R_Q$). Our data ($0.04 \leq (R_C/R_Q) \leq 0.4$) fully agree with this picture, and the non-superconducting phase is indeed always a weakly localizing metal.

As a conclusion, we showed that the superconducting O-2DEG at the LaTiO₃/SrTiO₃ interface undergoes a QPT from a superconductor to a weakly localizing metal (fermionic scenario) upon applying a perpendicular magnetic field, driven by phase fluctuations and well described by the (2+1)D XY model, as expected. By tuning the gate voltage, it is possible to explore the “clean” and “dirty” regimes according to the Harris criteria, with a critical exponents product $z\nu = 2/3$ in the former case, in agreement with previous evaluations[11][38], and greater than one otherwise. The system is well described by a disordered array of superconducting puddles coupled by a 2DEG, which can exhibit two QPT, one related to “regional” or local ordering, and another one corresponding to long range

phase coherence, as proposed theoretically[16–18]. The key parameter, that is the coupling constant (the 2DEG conductance), can be tuned at will to explore the phase diagram of the system. This is important in the context of recent studies of strongly disordered 2D superconductors where intrinsic inhomogeneities appear at mesoscopic scales[17, 39, 40], with coexistence of superconducting and non-superconducting regions. Recent work on artificial ordered metallic networks addresses this issue[41], but does not reach the insulating state. Our study opens the way for exploring the physics of disordered superconductors, and beyond, the more general problem of phase coherence in multiscale systems such as strongly correlated materials which are phase separated[42] or spin-textured[43].

The Authors gratefully thank C. di Castro, C. Castellani, L. Benfatto and C. Kikuchi-Marrache for stimulating discussions. This work has been supported by the Région Ile-de-France in the framework of CNano IdF and Sesame programs. Part of this work has been supported by Euromagnet II. Research in India was funded by the Department of Information Technology, Government of India.

-
- [1] Mannhart, J. & Schlom, D. G. Oxide Interfaces - An Opportunity for Electronics. *Science* **327**, 1607–1611 (2010).
- [2] Mannhart, J., Blank, D. H. A., Hwang, H. Y., Millis, A. J. & Triscone, J. M. Two-dimensional electron gases at oxide interfaces. *MRS bulletin* **33**, 1027–1034 (2008).
- [3] Hwang, H. Y. *et al.* Emergent phenomena at oxide interfaces. *Nature Mat.* **11**, 103–113 (2012).
- [4] Ohtomo, A. & Hwang, H. Y. A high-mobility electron gas at the LaAlO₃/SrTiO₃ heterointerface. *Nature* **427**, 423–426 (2004).
- [5] Brinkman, A. *et al.* Magnetic effects at the interface between non-magnetic oxides. *Nature Mat.* **6**, 493–496 (2007).
- [6] Shalom, M. B. *et al.* Anisotropic magnetotransport at the SrTiO₃/LaAlO₃ interface. *Phys. Rev. B* **80**, 140403 (2009).
- [7] Bert, J. A. *et al.* Direct imaging of the coexistence of ferromagnetism and superconductivity at the LaAlO₃/SrTiO₃ interface. *Nature Phys.* **7**, 767–771 (2011).
- [8] Li, L., Richter, C., Mannhart, J. & Ashoori, R. C. Coexistence of magnetic order and two-dimensional superconductivity at LaAlO₃/SrTiO₃ interfaces. *Nature Phys.* **7**, 762–766 (2011).
- [9] Reyren, N. *et al.* Superconducting interfaces between insulating oxides. *Science* **317**, 1196–1199 (2007).
- [10] Biscaras, J. *et al.* Two-dimensional superconductivity at a Mott insulator/band insulator interface LaTiO₃/SrTiO₃. *Nature Commun.* **1**, 89 (2010).
- [11] Caviglia, A., Gariglio, S., Reyren, N. & Jaccard, D. Electric Field Control of the LaAlO₃/SrTiO₃ Interface Ground State. *Nature* **456**, 624–627 (2008).
- [12] Biscaras, J. *et al.* Two-Dimensional Superconducting Phase in LaTiO₃/SrTiO₃ Heterostructures Induced by High-Mobility Carrier Doping. *Phys. Rev. Lett.* **108**, 247004 (2012).
- [13] Sondhi, S. L., Girvin, S. M., Carini, J. P. & Shahar, D. Continuous quantum phase transitions. *Rev. Mod. Phys.* **69**, 315–333 (1997).
- [14] Harris, H. B. Effect of random defects on the critical behaviour of Ising models. *J. Phys. C: Solid State Phys.* **7**, 1671–1692 (1974).
- [15] Goldman, A. M. Superconductor-Insulator Transitions. *Int. J. of Mod. Phys. B* **24**, 4081–4101 (2010).
- [16] Spivak, B., Zyuzin, A. & Hruska, M. Quantum superconductor-metal transition. *Phys. Rev. B* **64**, 132502 (2001).
- [17] Spivak, B., Oreto, P. & Kivelson, S. Theory of quantum metal to superconductor transitions in highly conducting systems. *Phys. Rev. B* **77** 214523 (2008).
- [18] Feigel'man, M. V., Larkin, A. I. & Skvortsov, M. A. Quantum superconductor-metal transition in a proximity array. *Phys. Rev. Lett.* **86**, 1869–1872 (2001).
- [19] Finkel'shtein, A. M. Superconducting transition temperature in amorphous films. *JETP Lett. (Pis'ma Zh. Eksp. Teor. Fiz.)* **45**, 46–49 (1987).
- [20] Yazdani, A. & Kapitulnik, A. Superconducting-insulating transition in two-dimensional a-MoGe thin films. *Phys. Rev. Lett.* **74**, 3037–3040 (1995).
- [21] Li, Y. H. & Teitel, S. Finite-Size Scaling Study of the 3-Dimensional Classical XY Model. *Phys. Rev. B* **40**, 9122–9125 (1989).
- [22] Ghosal, A., Randeria, M. & Trivedi, N. Role of spatial amplitude fluctuations in highly disordered s-wave superconductors. *Phys. Rev. Lett.* **81**, 3940–3943 (1998).
- [23] Goldman, A. M. & Marković, N. Superconductor-Insulator Transitions in the Two-Dimensional Limit. *Phys. Today* **51**, 39 (1998).
- [24] Kapitulnik, A., Mason, N., Kivelson, S. A. & Chakravarty, S. Effects of dissipation on quantum phase transitions. *Phys.*

- Rev. B* **63**, 125322 (2001).
- [25] Vishwanath, A., Moore, J. E. & Senthil, T. Screening and dissipation at the superconductor-insulator transition induced by a metallic ground plane. *Phys. Rev. B* **69**, 054507 (2004).
- [26] Biscaras, J. *et al.* Irreversibility and time relaxation in electrostatic doping of oxide interfaces. Preprint at <http://arxiv.org/abs/1206.1198> .
- [27] Fisher, M. P. A. Quantum phase transitions in disordered two-dimensional superconductors. *Phys. Rev. Lett.* **65**, 923–926 (1990).
- [28] Aubin, H. *et al.* Magnetic-field-induced quantum superconductor-insulator transition in $\text{Nb}_{0.15}\text{Si}_{0.85}$. *Phys. Rev. B* **73**, 094521 (2006).
- [29] Marrache-Kikuchi, C. *et al.* Thickness-tuned superconductor-insulator transitions under magnetic field in a-NbSi. *Phys. Rev. B* **78**, 144520 (2008).
- [30] Marković, N., Christiansen, C. & Goldman, A. Thickness-Magnetic Field Phase Diagram at the Superconductor-Insulator Transition in 2D. *Phys. Rev. Lett.* **81**, 5217–5220 (1998).
- [31] Kisker, J. & Rieger, H. Bose-glass and Mott-insulator phase in the disordered boson Hubbard model. *Phys. Rev. B* **55**, R11981–R11984 (1997).
- [32] Cha, M. C. & Girvin, S. M. Universal Conductivity in the Boson Hubbard-Model in a Magnetic-Field. *Phys. Rev. B* **49**, 9794–9801 (1994).
- [33] Mason, N. & Kapitulnik, A. Superconductor-insulator transition in a capacitively coupled dissipative environment. *Phys. Rev. B* **65** 220505 (2002).
- [34] Sørensen, E., Wallin, M., Girvin, S. & Young, A. Universal conductivity of dirty bosons at the superconductor-insulator transition. *Phys. Rev. Lett.* **69**, 828–831 (1992).
- [35] Steiner, M. A., Breznay, N. P. & Kapitulnik, A. Approach to a superconductor-to-Bose-insulator transition in disordered films. *Phys. Rev. B* **77**, 212501 (2008).
- [36] Bollinger, A. T. *et al.* Superconductor-insulator transition in $\text{La}_{2-x}\text{Sr}_x\text{CuO}_4$ at the pair quantum resistance. *Nature* **472**, 458–460 (2011).
- [37] Bert, J. A. *et al.* Gate-tuned superfluid density at the superconducting $\text{LaAlO}_3/\text{SrTiO}_3$ interface. *Phys. Rev. B* **86**, 060503 (2012).
- [38] Schneider, T., Caviglia, A. D., Gariglio, S., Reyren, N. & Triscone, J. M. Electrostatically-tuned superconductor-metal-insulator quantum transition at the $\text{LaAlO}_3/\text{SrTiO}_3$ interface. *Phys. Rev. B* **79**, 184502 (2009).
- [39] Sacépé, B. *et al.* Localization of preformed Cooper pairs in disordered superconductors. *Nature Phys.* **7**, 239–244 (2011).
- [40] Bouadim, K., Loh, Y. L., Randeria, M. & Trivedi, N. Single- and two-particle energy gaps across the disorder-driven superconductor-insulator transition. *Nature Phys.* **7**, 884–889 (2011).
- [41] Eley, S., Gopalakrishnan, S., Goldbart, P. M. & Mason, N. Approaching zero-temperature metallic states in mesoscopic superconductor-normal-superconductor arrays. *Nature Phys.* **8**, 59–62 (2011).
- [42] Dagotto, E. Complexity in Strongly Correlated Electronic Systems. *Science* **309**, 257–262 (2005).
- [43] Ruben, G., Morgan, M. & Paganin, D. Texture Control in a Pseudospin Bose-Einstein Condensate. *Phys. Rev. Lett.* **105**, 220402 (2010).

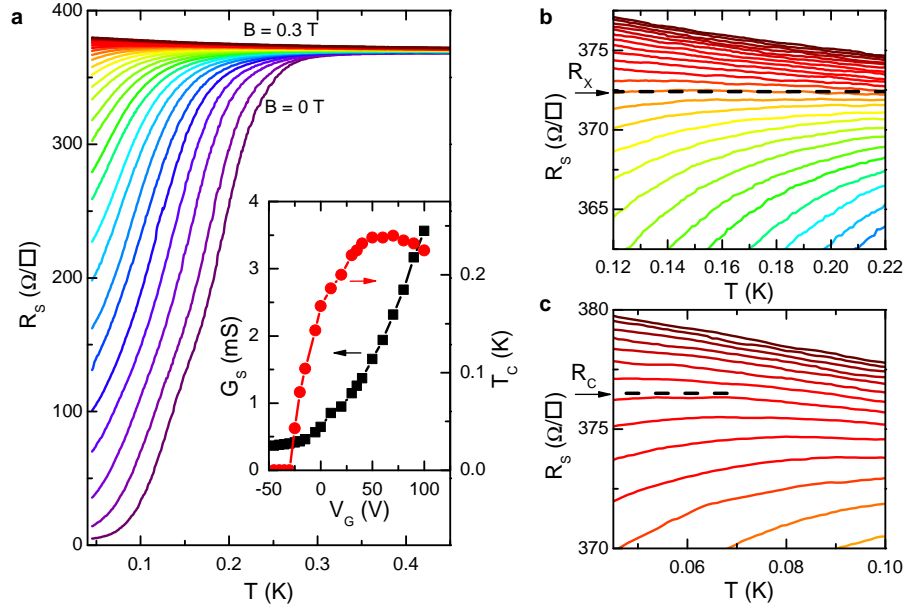


Figure 1: **Superconductor-insulator transition induced by a magnetic field.** **a**, Sheet resistance R_S as a function of temperature for different magnetic fields from 0 to 0.3 T. **Inset** : T_c and $G_S=1/R_S$ as a function of the gate voltage V_G . **b**, Zoom on the same data showing the characteristic magnetic field B_x , for which R_S is constant between 0.12 K and 0.22 K. **c**, Zoom on the same data showing the characteristic magnetic field B_c , which separates the two regimes at the lowest temperatures.

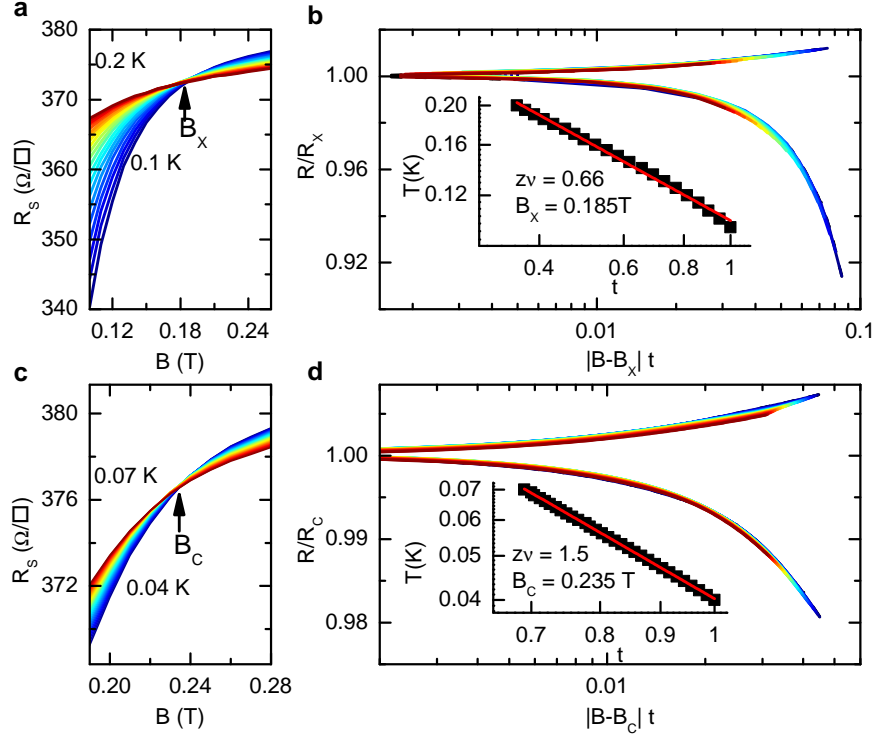


Figure 2: **Finite size scaling analysis for $V_G = +80$ V.** **a**, Sheet resistance R_s as a function of magnetic field B for different temperatures from 0.1 to 0.2 K. The crossing point is $(B_x=0.185$ T, $R_x=372.4$ Ω/\square). **b**, Finite size scaling plot R_s/R_x as a function of $|B - B_x|t$ (see text for the definition of t). **Inset** : temperature behaviour of the scaling parameter t . The power law fit gives $z\nu=0.66$. **c**, Sheet resistance R_s as a function of magnetic field B for different temperatures from 0.04 to 0.07 K ($V_G = +80$ V). The crossing point is $(B_C=0.235$ T, $R_C=376.6$ Ω/\square). **d**, Finite size scaling plot R_s/R_C as a function of $|B - B_C|t$. **Inset** : temperature behaviour of the scaling parameter t . The power law fit gives $z\nu=1.5$

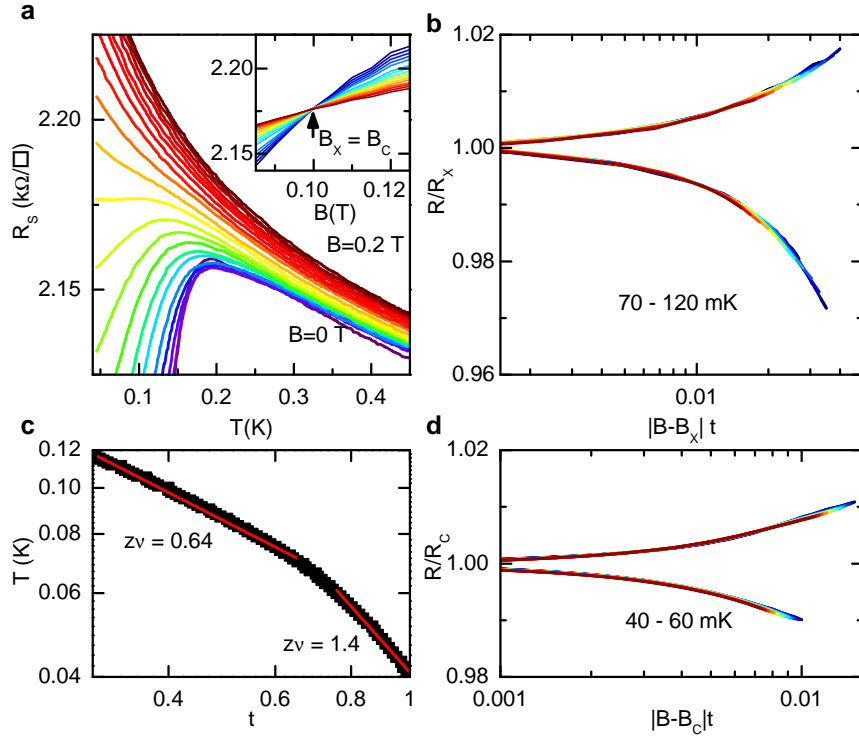


Figure 3: **Finite size scaling for $V_G = -15$ V.** **a**, Sheet resistance R_S as a function of temperature for different magnetic fields from 0 to 0.2 T. **Inset** : corresponding R_S as a function of the magnetic field for different temperatures from 0.07 K to 0.12 K. The crossing point is $(B_x=0.1$ T, $R_x=2176$ Ω/\square) . **b**, Temperature behaviour of the scaling parameter t : two distinct slopes are evidenced, 0.64 at high temperature and 1.4 at low temperature. **c**, Finite size scaling plot R_S/R_x as a function of $|B - B_x|t$ corresponding to the “high temperature” regime, with $z\nu=0.64$. **d**, Finite size scaling plot R_S/R_C as a function of $|B - B_C|t$ corresponding to the “low temperature” regime, with $z\nu=1.4$

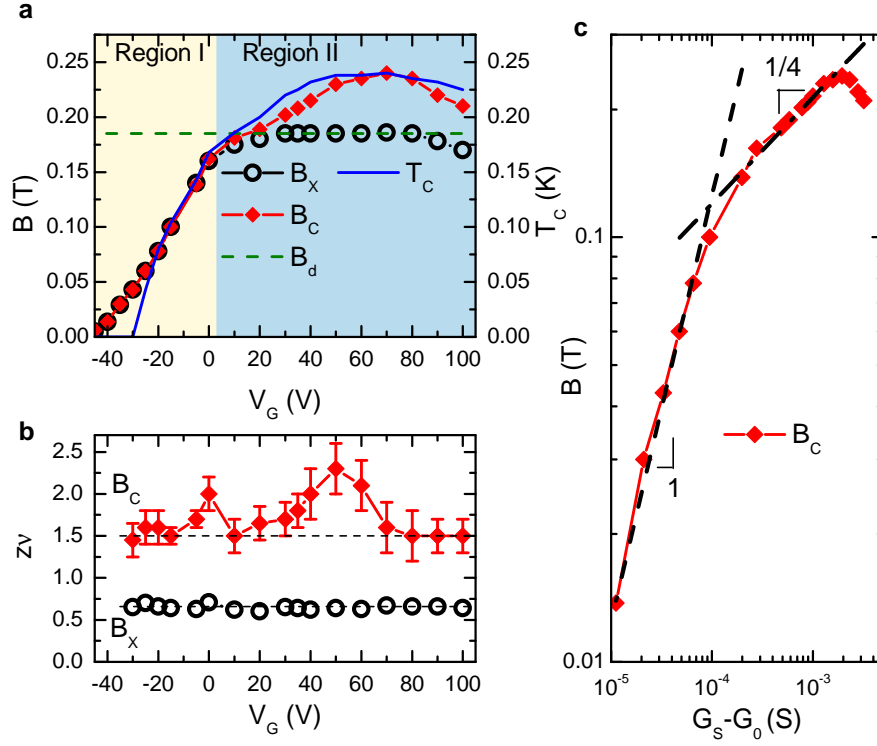


Figure 4: **The two quantum phase transitions.** **a**, B_x , B_C (left scale) and T_c (right scale) as a function of V_G . The dashed line corresponds to B_d (see text). Regions I and II refers to the low, and respectively high, coupling regimes (see text). **b**, $z\nu$ as a function of V_G for the two transitions (when $B_x=B_C$, B_C has been assigned to the “low temperature” regime, and B_x to the “high temperature” one). $z\nu$ is mainly constant with $z\nu=0.66$ for the “high temperature” transition. It is between 1.5 and 2.3 for the dirty one. The dashed lines correspond to $z\nu=2/3$ and $z\nu=3/2$. **c**, B_C as a function of G_S on a log scale. Dashed lines have slopes 1 and 1/4 respectively as expected from the SOK model.

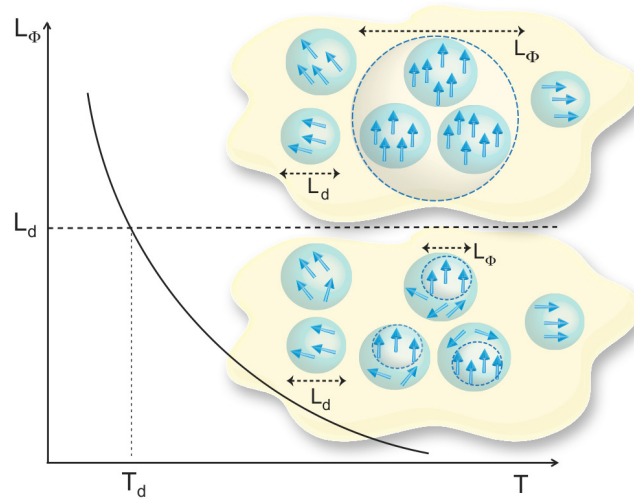


Figure 5: **Sketch of the role of mesoscopic disorder on the QPT.** The dephasing length L_Φ diverges with temperature, and reaches the size of the superconducting puddles L_d at T_d . The insets show a piece of material in the two regimes. At high temperature (bottom), $L_\Phi < L_d$ and the system is in the clean limit, whereas at low temperature (top), $L_\Phi > L_d$, and the system is in the dirty limit. In this drawing, superconducting puddles (in blue) are coupled through a 2DEG (in yellow). The arrows symbolize the local phase of the superconductor